Specimen-induced aberrations and adaptive optics for microscopy

Martin J. Booth, Michael Schwertner and Tony Wilson

Department of Engineering Science, University of Oxford, U.K.

ABSTRACT

The imaging properties of optical microscopes can be severely compromised by specimen-induced aberrations causing degraded resolution, reduced signal levels, and image distortion. This is particularly the case in high-resolution, three-dimensional techniques, such as scanning confocal or multi-photon fluorescence microscopy - techniques used extensively in the biological sciences. The aberrations are caused by spatial variations of refractive index within the specimen itself. In wide-field microscopes, this gives rise to aberrations that change across the field of view; in scanning microscopes, they cause temporal variations as the focal spot is scanned through the specimen. The application of adaptive optics to this problem has obvious potential and the principle has been demonstrated in scanning microscopes. To characterise the optical properties of specimens and determine the requirements for adaptive microscopes, we have performed the first detailed study of biological specimen-induced aberrations using an interferometer incorporating high NA microscope objectives. We show that low order correction of aberrations produces significant recovery of signal and resolution and we compare the performance of different correction devices, e.g. deformable and segmented mirrors, for imaging such specimens. It is also shown that that the presence of tip, tilt and defocus modes leads to three-dimensional image distortion that is not easily removed by an adaptive correction system.

Keywords: Microscopy, confocal microscopy, aberrations, wave front sensing, Zernike polynomials, adaptive optics

1. INTRODUCTION

Optical microscopes, including the confocal fluorescence microscope (CFM) and the two-photon excitation fluorescence microscope (or two-photon microscope - TPM), have become standard instruments in many life science laboratories.[1–3] Modern microscopes are highly optimised and are designed to deliver performance close to the physical diffraction limit. However, there is one element in the optical path that has a strong influence on the image quality but is hard to optimise: the specimen itself. A biological specimen may have, apart from absorption properties, a variation in refractive index. If one intends to image details within a cell, the distribution of the refractive index in the obstructing layers above the focal region introduces aberrations. Aberrations have been subject to many investigations due to their detrimental effect on imaging quality.[4–9] In CFM and TPM aberrations lead to reduced resolution and lower signal levels. It is clearly desirable to compensate for these effects in order to restore imaging quality.

We describe the measurement and quantification of specimen induced aberrations from a number of biological specimens. Furthermore, using the examples of a CFM and TPM, we investigate the viability of low order aberration correction in high numerical aperture (NA) microscopy and the expected improvement in signal levels. We discuss the development of adaptive optics technologies for use in microscopy issues affecting the choice of aberration correction devices.

Further author information:
E-mail: martin.booth@eng.ox.ac.uk
Full address: Department of Engineering Science, University of Oxford, Parks Road, Oxford, OX1 3PJ, United Kingdom

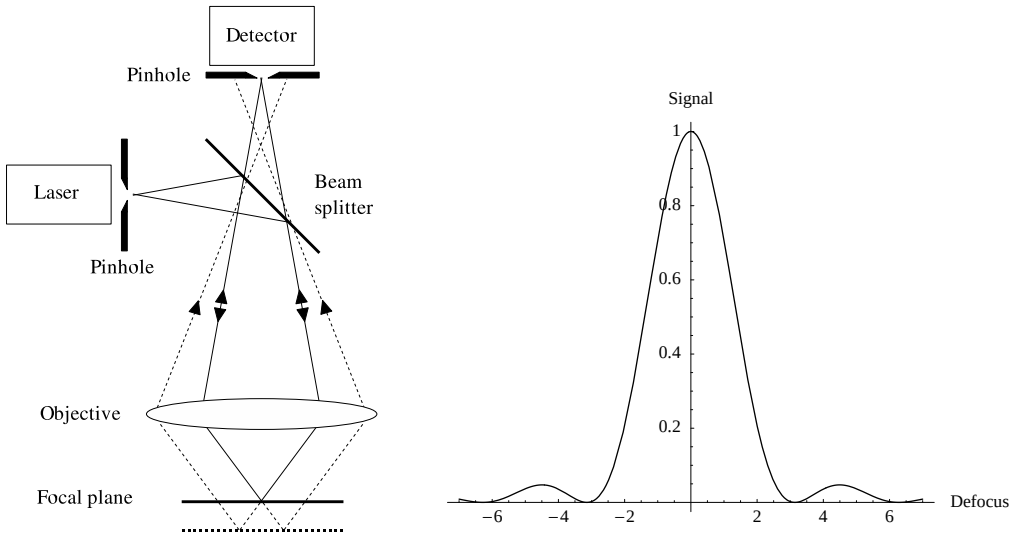

Figure 1. The principle of operation of a confocal microscope. When a plane reflector is placed in the focal plane, most of the reflected light passes through the detection pinhole. When the reflector is moved out of the focal plane, the light no longer reaches the detector but is obscured by the pinhole screen. The graph shows the detector signal as the reflector is defocussed (normalised units).

2. CONFOCAL AND MULTI-PHOTON MICROSCOPY

The scanning confocal microscope is an important tool for many imaging applications, particularly in biomedical science.[1–3] Its strength lies in its ability to create three dimensional representations of volume object at high resolution. Many commercial instruments are available that typically offer a variety of imaging modes including brightfield, fluorescence and two photon excitation fluorescence. The principle of operation of the reflection mode confocal microscope is illustrated in Figure 1. A point-like laser light source is focussed by the objective lens into the specimen where it is scattered or reflected by specimen features. In this *epi*-configuration, the light passes back through the same objective lens, which forms part of an optical system that images the focal spot onto a pinhole placed in front of a photodetector. The image is constructed point by point by scanning the specimen in three-dimensions relative to the focal spot. This imaging configuration results in improved lateral resolution, compared to the conventional microscope, and also demonstrates powerful axial sectioning. The reason for this sectioning strength can be seen in Figure 1: only light scattered from the focal plane totally passes through the detection pinhole and contributes to the signal; light scattered from other parts of the specimen falls mainly upon the opaque screen and only a negligible proportion passes through the pinhole. The sectioning property allows three dimensional imaging: data can be taken from a sequence of planes within the sample and then be reconstructed by software into a three dimensional rendering.

The principle of operation of the CFM is similar: light from a laser is focussed by an objective lens into the specimen, where it excites fluorophores that either may be a natural part of the specimen or deliberately introduced as a contrast mechanism. This excitation occurs not only in the focal region but also throughout the illumination cone. The fluorescent emission is then collected by the same objective lens and passes through a dichroic beamsplitter that separates the emission light from the excitation light. The pinhole obscures fluorescent light emitted from outside of the focal region thus providing three-dimensional resolution and superior image contrast in comparison with conventional fluorescence microscopes.

The CFM relies upon a single photon absorption process whereby a photon is absorbed by a fluorophore, which then re-emits a photon of lower energy. In a TPM the fluorescence is generated by the simultaneous absorption of two, longer wavelength photons with sufficient total energy to excite the fluorophore.[10] However, the two photon excitation probability is proportional to the square of the illumination intensity and is much less efficient that single photon absorption. Therefore, TPMs usually employ short pulsed femtosecond lasers

to increase fluorescence yields. The non-linear dependence of the fluorescence generation on the illumination intensity means that fluorescence is only generated in the focal region. The TPM therefore has intrinsic optical sectioning, even when a pinhole is not placed before the detector.

3. ADAPTIVE OPTICS FOR MICROSCOPY

The effects of aberrations on the imaging quality of confocal microscopes have been extensively investigated because they fundamentally limit the final image resolution and signal level.[11–15] This fact may be understood by considering an object point located at a certain depth below the surface of the specimen. Fluorescence must first be excited at this point by a well focussed, diffraction-limited spot of light. It is then necessary to reimage the excited volume back through the specimen and the rest of the optical system to the detection pinhole. Any imperfections, however introduced, will cause spreading of the focussed spot and will inevitably lead to a reduction in signal level, as well as impaired imaging. One of the major sources of imperfection is that of specimen-induced spherical aberration. This aberration occurs, for example, when focussing through an interface between materials of different refractive index. Such refractive index mismatches occur between the immersion medium, the coverglass, and the specimen. The specimen may introduce further aberrations if it consists of regions of differing refractive index. In general, aberrations cause a reduction in lateral resolution and, more significantly, degrade the axial resolution and cause a fall in signal intensity. As the aberrations increase, for example, when focussing deeper into a specimen, the image contrast rapidly deteriorates. The specimen itself can therefore limit the useful focussing depth.

The restoration of signal level through aberration correction is particularly important. Optical efficiency is of primary relevance in biological fluorescence microscopy, especially for live cell imaging, where low illumination powers and fluorophore concentrations are required to limit toxic effects in the specimen. A further problem arises due to photobleaching, whereby fluorescent molecules are changed into a non-fluorescent state and the fluorescence yield gradually decreases to zero. This process is exacerbated by the higher illlumination intensities that one might employ to counteract the effect. The efficient detection of fluorescence photons and the restoration of signal level through aberration correction are therefore important goals in the design of a microscope.

Aberrations can be removed using adaptive optics, a concept which is widely used in astronomy where aberrations are introduced by refractive index variations in the atmosphere.[16] In microscopy, one attempts to image through an obstructing volume of inhomogeneous refractive index and possibly layers of mismatched refractive index. The idea of adaptive optics is to introduce conjugate aberrations that cancel out the aberrations arising within the system, thus recovering optimum, diffraction limited imaging. The principle of adaptive aberration correction has been demonstrated within a TPM.[17–19] A more efficient implementation was incorporated into a CFM,[20] where a single deformable mirror was used for both wave front sensing and correction employing a modal wave front sensing technique.[21, 22]

4. CHARACTERISATION OF SPECIMEN-INDUCED ABERRATIONS

There have been several theoretical investigations that were primarily concerned with spherical aberration arising from refractive index mismatch.[4–9] However, biological specimens can have complicated variations in refractive index. The average refractive index of tissue or the refractive index of particular regions of biological specimens has been previously been investigated.[11, 12] More recently, the form and magnitude of aberrations introduced by complex biological specimens have been measured.[13–15] This information is essential for a systematic and directed approach to the design of an adaptive optical microscope. In this Section, we describe measurements of aberrations induced by biological specimens and we outline methods for their characterisation.

4.1. Interferometric measurement of specimen-induced aberrations

We built a Mach-Zehnder phase stepping interferometer (Figure 2) to measure the aberrations induced by various specimens.[15] The expanded He-Ne (633 nm) laser beam was split into reference and object paths. The specimen was placed in the object path between two opposing water immersion lenses (Carl Zeiss C-Apochromat, 63x Korr, NA=1.2) that were equipped with cover glass correction collars. A rotation of the $\lambda/2$-plate in front of the polarising beamsplitter permitted the adjustment of the relative intensities of the two interferomter paths.

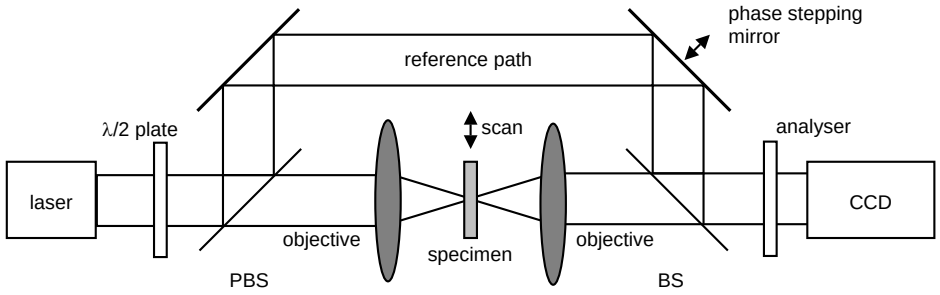

Figure 2. Schematic of the phase stepping interferometer for aberration measurement. (PBS - polarising beam splitter, BS - beam splitter.) The specimen is mounted between two opposing high NA lenses and scanned laterally by means of a computer controlled stage. Some intermediate lenses have been omitted for clarity.

When the object beam traversed the specimen it was made to interfere with the reference beam and the resulting interference pattern was recorded on a CCD camera. The image plane of the CCD was conjugate to the pupil plane of the second objective lens. The phase stepping unit placed in the reference beam path took the form of a flat mirror mounted on a calibrated piezo drive. This allowed us to change the relative phase between reference and object beams in well defined steps. The phase stepping was synchronised with the CCD-camera and digital interferogram images were recorded using a framegrabber. The specimen was attached to a piezo driven stage that could be positioned in three dimensions. Furthermore, for specimen navigation, the object path could be switched to operate as a conventional transmission microscope using an additional CCD camera and illumination elements (not shown in the Figure). Aberrations can be modelled by a complex pupil function

$$P(r,\theta) = A(r,\theta)\exp(j\psi(r,\theta)) \tag{1}$$

where $A(r,\theta)$ denotes the amplitude, $\psi(r,\theta)$ is the phase and $j = \sqrt{-1}$. Using the phase stepping interferometer, we acquired a set of three interferograms at different relative phase steps and measured $A(r,\theta)$ and the wrapped phase function $\phi(r,\theta)$, where[13]

$$\phi(r,\theta) = \psi(r,\theta) \bmod 2\pi. \tag{2}$$

The wave front phase $\psi(r,\theta)$ could then be recovered from $\phi(r,\theta)$, for example, using a phase unwrapping technique.[15,23] Example wave fronts from six different specimens are shown in Figure 3.

4.2. Analysis of aberration effects

A convenient way to describe the aberrations is a series of Zernike polynomials, so that the phase is expressed as the summation $\psi(r,\theta) = \sum_i M_i Z_i(r,\theta)$.[24,25] The Zernike mode amplitudes, M_i, can be extracted from the unwrapped phase as

$$M_i = \frac{1}{\pi}\int_0^1 \int_0^{2\pi} \psi(r,\theta) Z_i(r,\theta)\, r\mathrm{d}\theta\mathrm{d}r. \tag{3}$$

Throughout this paper we use the indexing and normalization scheme of the Zernike polynomials as used by Schwertner *et al.* where all polynomials for $i > 1$ have a standard deviation of one radian over the unit circle.[13] We can separate the Zernike modes into two classes: the first set consists of the Zernike modes tip ($i = 2$), tilt ($i = 3$) and defocus ($i = 4$). In a CFM they simply produce a displacement of the focal spot from its nominal position within the specimen. However, the image of the focal spot always falls on the pinhole detector since a conjugate displacement is introduced when the spot is re-imaged via the aberrating medium. In a sense, these modes are self correcting in an *epi*-mode CFM but the displacement between the actual and nominal focal position in the specimen causes geometric distortion in the acquired three-dimensional image which can influence the accuracy of spatial measurements. The second class of modes ($i > 4$) changes the shape of the intensity distribution in the focal region and influences signal level and resolution.

The quality of an optical system is often characterised by the Strehl ratio, S, which is defined as the ratio of the maxima of the focal intensity distributions for the aberrated and the unaberrated system.[24] For moderate

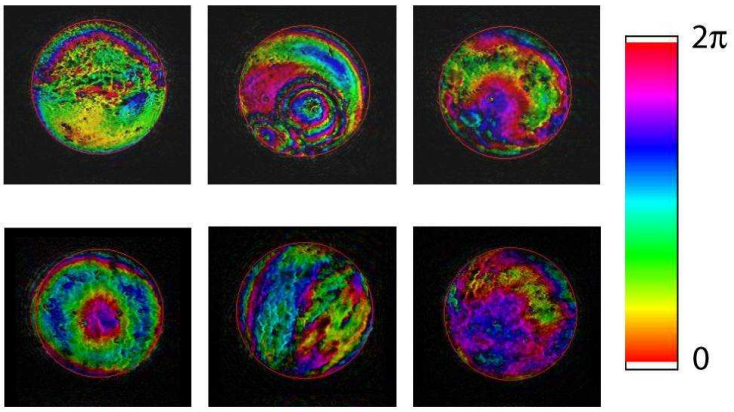

Figure 3. Example complex wave fronts acquired from six different specimens. Top row: rat brain, mouse oocyte and rat liver. Bottom row: rat heart muscle, c. elegans and rat smooth muscle. The colour encodes the phase of the wave front whereas the brightness represents the amplitude (colour only in the electronic version).

aberrations and especially if the wave front contains only small amounts of the Zernike modes tip, tilt or defocus, then S is equivalent to the ratio of the intensity at the nominal focus to the diffraction limited maximum intensity. For small aberrations and no amplitude variations the Strehl ratio may be estimated from the variance of the wave front and finally the Zernike mode coefficients M_i as[24]:

$$S \approx 1 - \mathrm{Var}(\psi(r,\theta)) = 1 - \sum_{i=5}^{\infty} M_i^2. \tag{4}$$

This is valid for $\mathrm{Var}(\psi(r,\theta)) \ll 1$. In both CFM and TPM systems, within reasonable approximations, the maximum signal detected from a point-like fluorescence object is proportional to the square of the Strehl ratio.[15] Calculation of S^2 therefore provides us with an estimate of the effect that the measured aberrations have on fluorescence signal levels. We can also define the signal improvement factor, F_{sig}, for a CFM or TPM system to be:

$$F_{sig} = \left(\frac{S_{corr}}{S_{ini}} \right)^2. \tag{5}$$

Here S_{ini} denotes the initial Strehl ratio of the uncorrected wave front and S_{corr} the Strehl ratio of the corrected wave front. The value of F_{sig} represents the improvement in signal when aberration correction is applied to the excitation path of a TPM or the excitation and emission paths of a CFM using an infinitely small pinhole. This model of the imaging process allows us to estimate the potential benefit of adaptive optics in a straightforward manner. For small but finite sized pinholes in CFM, F_{sig} is expected to be similar. We note that the Zernike coefficients have units of phase and are therefore dependent upon wavelength. If no dispersion is present, the measured Zernike coefficients scale inversely with the wavelength. In this case it would be a simple matter to recalculate the factor of improvement for other wavelengths. Figure 4 shows the distribution of S_{ini}, S_{corr} and F_{sig} for regions of six different specimens. The results shown assume an excitation wavelength of 633nm. It can be seen that, after correction of Zernike modes 5 to 22, the fluorescence signal increases by a significant factor across large proportions of the specimen. We note that this increase in signal is not necessarily concomitant with a corrected Strehl ratio near the diffraction limit, since residual aberrations may be present.

The Zernike modes tip, tilt and defocus are self-correcting in the CFM and TPM and hence do not affect the detected signal level but do cause distortion of the three-dimensional image. This is of obvious importance in situations where one wishes to measure the relative position of features in the specimen. Furthermore, it is

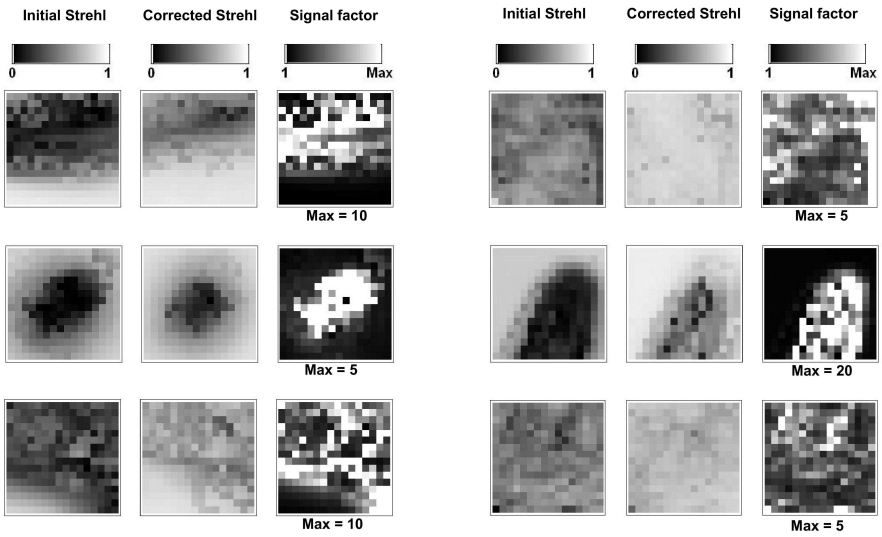

Figure 4. Initial and corrected Strehl ratios and signal factor for correction of Zernike modes 5 to 22. The six specimens are: rat brain, mouse oocyte and rat liver (left column from top to bottom); rat heart muscle, c. elegans and rat smooth muscle (right column from top to bottom).

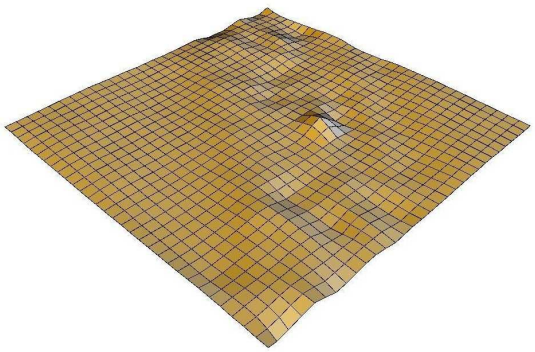

Figure 5. Simulated distortion of a 32×32μm grid placed below a region of a c. elegans specimen. The maximum lateral displacement was 0.2μm and the maximum axial displacement was 0.9μm.

important to note that a wave front sensor in an *epi*-mode microscope would not be able to measure the tip, tilt and defocus components. Using the interferometric data sets, we have simulated the distortion induced in the image of a planar grid object placed below the specimen (Figure 5). Each point on the grid is displaced along three axes according to the corresponding tip, tilt and defocus measurements. These results show that in an *epi*-mode CFM or TPM system where all higher order aberrations are corrected, there could still be image distortion present.

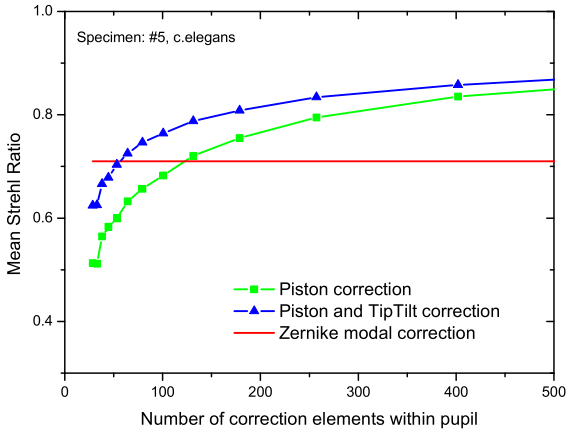

Figure 6. Comparison of the correction efficiency of different DM devices for imaging the c. elegans specimen. The horizontal line represents the level of correction provided by perfect correction of Zernike modes 5 to 22. The performance of the segmented devices was modelled for different numbers of correction elements within the pupil. The vertical axis shows the mean, corrected Strehl ratio for the whole data set.

5. ABERRATION CORRECTION IN MICROSCOPY

In the CFM, aberrations are introduced in two ways: firstly, the illumination light passes through the inhomogeneous refractive index distribution in the specimen, focussing to an aberrated focal spot; secondly, as the focal fluorescence emission is imaged by the optical system onto the detector pinhole, further aberrations are introduced. Since the illumination light and emission light pass through the same part of the specimen, the optical path length aberrations are equivalent. A single aberration correction device can therefore be used to correct both paths. Deformable mirrors are ideally suited to this task because of their high optical efficiency and wavelength independence. Liquid crystal SLMs are less suited to the task due to their lower optical efficiency and wavelength and polarisation dependence. In the TPM, it is not necessary to use a detector pinhole and aberration correction is therefore only essential in the illumination path. Again, deformable mirrors are best suited to the task, although SLMs have also been employed.[26]

Using the interferometric measurements of specimen-induced aberrations, we have modelled and compared the correction efficiencies of different DM devices for use in the CFM and the TPM. In the previous Section, we modelled correction based upon the removal of the low-order Zernike modes (modes 5 to 22) - this is approximately equivalent to the capabilities of presently available, continuous surface DMs.[27,28] We have also modelled the use of segmented DMs of two types: i) a DM consisting of independent piston correction elements; ii) a DM with independent tip/tilt/piston correction elements. In each case, the elements were arranged in a square grid pattern and the device was assumed to have 100% fill-factor. Figure 6 shows the results for one particular specimen. We note that for each element in the tip/tilt/piston DM there would be three degrees of freedom, requiring at least three independent actuators, whereas in the piston-only DM there would be one actuator per element. We examined a range of specimens and found the number of elements for both devices that were required to provide a Strehl ratio equivalent to the modal correction. It was found that the required number varied considerably between specimens, indicating that the optimum choice of correction devices might depend upon the specimen.

6. CONCLUSION

Specimen induced aberrations lead to reduced signal levels and a deterioration in image quality in optical microscopy, especially in CFM and TPM. We have classified and quantified specimen induced aberrations introduced by various biological specimens. The approach can provide detailed information about the variation of each Zernike coefficient during imaging. This could also deliver information about the temporal dynamics of the aberrations due to the scanning of the focal spot through the specimen. Our calculation of the correction benefit is based on the assumption that a correction would be applied at every position within the scanned area. The feasibility of this assumption depends on the bandwidth of the wave front sensing and correction devices and the scan speed. In some cases it may be required to either reduce the scan speed or update the aberration correction every few pixels only. The measurements indicate significant variations of the uncorrected Strehl ratio throughout the specimen. We showed that low order aberration correction based on Zernike modes will provide significant recovery of signal levels in CFM and TPM, even if the diffraction limit is not restored. The results presented here quantify the benefit of adaptive optics for biological microscopy and provide the bounds within which these systems must operate.

7. ACKNOWLEDGEMENTS

This work was supported by the Research Councils UK under the Basic Technology scheme. M.J.B. is a Royal Academy of Engineering / EPSRC Research Fellow. M.S. is supported by the DAAD Germany (German Academic Exchange Service).

REFERENCES

1. T. Wilson and C. J. R. Sheppard, *Theory and Practice of Scanning Optical Microscopy*, Academic Press, London, 1984.
2. T. Wilson, ed., *Confocal Microscopy*, Academic Press, London, 1990.
3. J. B. Pawley, ed., *Handbook of Biological Confocal Microscopy*, Plenum, New York, 1995.
4. S. Hell, G. Reiner, C. Cremer, and E. Stelzer, "Aberrations in confocal fluorescence microscopy induced by mismatches in refractive index," *J. Microsc.* **169**(3), pp. 391–405, 1993.
5. T. Wilson and A. R. Carlini, "The effects of aberrations on the axial response of confocal imaging systems," *J. Microsc.* **154**(3), pp. 243–256, 1989.
6. M. J. Booth, M. A. A. Neil, and T. Wilson, "Aberration correction for confocal imaging in refractive-index-mismatched media," *J. Microsc.* **192**(2), pp. 90–98, 1998.
7. M. J. Booth and T. Wilson, "Strategies for the compensation of specimen induced aberration in confocal microscopy of skin," *J. Microsc.* **200**(1), pp. 68–74, 2000.
8. P. Török, P. Varga, Z. Laczik, and G. R. Booker, "Electromagnetic diffraction of light focused through a planar interface between materials of mismatched refractive indices: an integral representation," *J. Opt. Soc. Am. A* **12**, p. 325, 1995.
9. P. Török, P. Varga, and G. Németh, "Analytic solution of the diffraction integrals and interpretation of wave-front distortion when light is focussed throug a planar interface between materials of mismatched refractive indices," *J. Opt. Soc. Am. A* **12**, pp. 2660–2671, 1995.
10. W. J. Denk, J. P. Strickler, and W. W. Webb, "Two-photon laser scanning fluorescence microscopy," *Science* **248**, pp. 73–76, 1990.
11. F. P. Bolin, L. E. Preuss, R. C. Taylor, and R. J. Ference, "Refractive index of some mammalian tissues using a fiber optic cladding method.," *Applied Optics* **28**(12), pp. 2279–2303, 1989.
12. G. J. Tearney, M. E. Brezinski, J. F. Southern, B. E. Bouma, M. R. Hee, and J. G. Fujimoto, "Determination of the refractive index of highly scattering human tissue by optical coherence tomography.," *Optics Letters* **20**(21), pp. 2258–2260, 1995.
13. M. Schwertner, M. J. Booth, M. A. A. Neil, and T. Wilson, "Measurement of specimen-induced aberrations of biological samples using phase stepping interferometry," *J. Microsc.* **213**(1), pp. 11–19, 2004.
14. M. Schwertner, M. J. Booth, and T. Wilson, "Simulation of specimen induced aberrations for objects with spherical and cylindrical symmetry," *J. Microsc.* **215**(3), pp. 271–280, 2004.

15. M. Schwertner, M. J. Booth, and T. Wilson, "Characterizing specimen induced aberrations for high NA adaptive optical microscopy," *Optics Express* **12**(26), pp. 6540–6552, 2004.
16. J. W. Hardy, *Adaptive Optics for Astronomical Telescopes*, Oxford University Press, 1998.
17. M. A. A. Neil, M. J. Booth, and T. Wilson, "Closed-loop aberration correction by use of a modal Zernike wave-front sensor," *Opt. Lett.* **25**(15), pp. 1083–1085, 2000.
18. L. Sherman, J. Y. Ye, O. Albert, and T. B. Norris, "Adaptive correction of depth-induced aberrations in multiphoton scanning microscopy using a deformable mirror," *J. Microsc.* **206**(1), pp. 65–71, 2002.
19. P. N. Marsh, D. Burns, and J. M. Girkin, "Practical implementation of adaptive optics in multiphoton microscopy," *Optics Express* **11**, pp. 1123–1130, 2003.
20. M. J. Booth, M. A. A. Neil, R. Juškaitis, and T. Wilson, "Adaptive aberration correction in a confocal microscope," *Proc. Nat. Acad. Sci.* **99**(9), pp. 5788–5792, 2002.
21. M. A. A. Neil, M. J. Booth, and T. Wilson, "New modal wavefront sensor: a theoretical analysis," *J. Opt. Soc. Am. A* **17**(6), pp. 1098–1107, 2000.
22. M. J. Booth, "Direct measurement of Zernike aberration modes with a modal wave front sensor," *Proc. S.P.I.E., 'Advanced Wavefront Control: Methods, Devices, and Applications'* **5162**, pp. 79–90, 2003.
23. D. C. Ghiglia and M. D. Pritt, *Two Dimensional Phase Unwrapping. Theory, Algorithms and Software.*, Wiley, 1998.
24. M. Born and E. Wolf, *Principles of Optics*, Pergamon Press, 6th ed., 1983.
25. R. Noll, "Zernike polynomials and atmospheric turbulence," *J. Opt. Soc. Am.* **66**, pp. 207–277, 1976.
26. M. A. A. Neil, R. Juškaitis, M. J. Booth, T. Wilson, T. Tanaka, and S. Kawata, "Adaptive aberration correction in a two-photon microscope," *J. Microsc.* **200**(2), pp. 105–108, 2000.
27. G. Vdovin, P. M. Sarro, and S. Middelhoek, "Technology and applications of micromachined adaptive mirrors," *Journal of Micromech. and Microeng.* **9**(2), p. R8, 1999.
28. N. Doble, G. Yoon, L. Chen, P. Bierden, B. Singer, S. Olivier, and D. R. Williams, "Use of a microelectromechanical mirror for adaptive optics in the human eye," *Optics Letters* **27**(17), pp. 1537–1539, 2002.